Study of dimensionless quantities to analyse front and rear wall of keyhole formed during laser beam welding

N KUMAR*, S DASH, A K TYAGI and BALDEV RAJ

Surface and Nanoscience Division, Indira Gandhi Centre for Atomic Research, Kalpakkam 603 102, India
e-mail: niranjan@igcar.gov.in

Abstract. Fluid flow mechanisms present in Keyhole (KH) during Laser Beam Welding (LBW) process influence the associated heat and mass transfer. In an attempt to describe these complexities for eventual optimization of LBW parameters, a dimensionless analysis using Mach (Ma), Raleigh (Ra), Reynolds (Re) and Marangoni (Mg) numbers have been carried out. This analysis describes hydrodynamics of melt and vapour phase appearing in the front and rear wall of KH. The non-dimensional hydrodynamic quantities describe the mechanism behind flow pattern present in melt-vapour in terms of ratio of convection–conduction heat transfer occurring within KH. The analysis shows that the higher Marangoni number indicates stronger Marangoni convection in the KH causing relatively higher capillary flow in the melt pool. The laminar-turbulent flow of melt-vapour in KH medium is described in terms of ratio of Reynolds and Mach numbers (Re/Ma). The pressure distribution in the KH accounts for the melt-vapour ejection rate. A relationship between depth and radius of KH has been obtained as a function of delivered laser power.

Keywords. Keyhole; weld pool; hydrodynamics; non-dimensional quantities; vapour pressure.

1. Introduction

There are several reports in literature which deal with melt pool hydrodynamics prevailing inside KH during LBW (Duley 1999; Kroos *et al* 1993; Kaplan 1994; Solana & Negro 1997; He *et al* 2003; De *et al* 2003; Trivedi *et al* 2007). Above a certain value of laser power density exceeding 10^6 Wcm^{-2}, the vapour recoil pressure burst causes the cavity transverse section appear like a KH. The material upon high power laser impact, vapourizes instantaneously from the molten region. This sudden burst of vapour pressure expels molten metal along the walls of the cavity. The vapour pressure in the front wall of the KH is always higher than that at the rear wall of the KH. This leads to higher pressure dissipation in the rear wall of the KH. The surface tension

---

*For correspondence

pressure tends to close the KH while the recoil pressure always acts to expose it. Model calculations show that when the KH diameter is of the same order as the sheet thickness, the latter part can become dominant, causing the KH to elongate. Existing models of the pressure balance cannot explain KH elongation dynamics described by Kroos *et al* (1993). The KH is surrounded by a pool of molten metal. The interface between the KH and melt pool is a freely moving surface. The quasi-static behaviour of the KH is studied by considering the pressure balance at this surface shown by He *et al* (2003) and Trivedi *et al* (2007). The transmission direction of the reflected laser power on the inclination angle of the KH front depends on the welding velocity and the local laser intensity. The reflected beam may have any direction. At low welding velocities (or high laser intensities), the reflected beam is directed downwards and is transmitted through the sheet. At high welding velocities (or low laser intensities), it is directed upwards and thus no bottom aperture of the KH is generated. It is interesting to note that for operating conditions where the rear wall of KH inclination attains 45°, the reflected beam runs parallel to the target surface. The rear wall of KH then directly gets irradiated by this reflected beam. If incident laser intensity is sufficiently high, the rear wall of KH is efficiently ejected. This effect occurs for a welding speed of about 8–10 m/min at 3 kW laser power described by Fabbro *et al* (2005). The 3-D modelling study shows that besides the welding speed, Marangoni convection and natural convection may affect the melt flow and temperature distribution in full-penetration LBW. The predicted relationship between the Nusselt number (characterizing the laser power absorbed by the work piece) and the Peclet number (dependent on welding speed) can be used to estimate the KH radius or evaluate the energy efficiency in full-penetration LBW (Xiao-Hu & Xi Chen 2002). In the simulation, the KH is formed by the displacement of the melt induced by evaporation recoil pressure while surface tension and hydrostatic pressure counteracts cavity formation. A transition mode having the geometry of the conduction mode with KH formation occurs in between conduction and KH modes. Initiation of the protrusion is caused mainly by collision of upward and downward flows due to the pressure components. Marangoni flow is known to have a minor effect on the flow patterns and KH stability. While high recoil pressure is exerted on the KH, especially at the bottom, it is not sufficient to eject the melt entirely out of the cavity as the upward flow momentum from the KH bottom is reduced by the viscous shear stress present on the KH wall (Lee *et al* 2002). Although dimensionless parameters have been extensively useful to understand transport phenomena of melt-vapour laden KH, a comprehensive hydrodynamic picture of their role at KH extremities is still a matter of study (Kumar *et al* 2007). The melt hydrodynamics is important which may influence the microstructure of weld pool its durability and strength.

   The present paper attempts to address non-dimensional mechanism of melt-vapour motion at front and rear wall of KH extremities in a typical experiment pertaining to LBW of Al 1100 alloy which considers pressure balance inside KH.

2. Experimental

The welding conditions of aluminum and its alloys are influenced by their oxidation characteristics. Physical property of the oxide layer also plays an important role. In addition, thermal, electrical and mechanical properties and melting characteristics need to be considered. LBW is considered to be a viable fusion joining process for aluminum through utilization of high-power laser systems. Effective coupling of the laser beam with relatively high power densities are advantageous factors. In the present study, high-power CW CO_2 laser is used to produce deep penetration welds at high welding speeds. The laser works at maximum power of 6 kW

Figure 1. Laser used in experiment during laser welding.

with wavelength of 10.64 μm in continuous mode (figure 1). The laser power supply is capable of delivering laser light that has accurate and repeatable energy and duration. When the laser beam is focused into a small spot adjustable approximately 0.1 to 0.8 mm in diameter onto the workpiece, the energy density becomes quite large. The light is absorbed by the metal, causing a 'keyhole' effect as the focused beam 'drills' into, vapourizes and melts some of the metal. As the sample moves, the liquefied metal around the 'keyhole' flows back in, solidifying and creating a small spot weld. The entire process takes only milliseconds. Although most metals get successfully welded, there are several difficulties in LBW processing of aluminum alloys. High thermal diffusivity of aluminum alloys and optical reflectivity of CW CO_2, laser radiation causes difficulty in coupling the laser energy to the material. Much higher laser intensities are required to ensure adequate coupling so that KH is not only formed but also remain hydrodynamically stable. These conditions allow formation of smooth fusion zone. Absorption of laser energy improves significantly with KH formation. However, laser welds in aluminum alloys contain excessive porosity. Differential vapourization of alloying elements also occur in the fusion zone. In a typical experiment, LBW of structural aluminum Al 1100 with varying thicknesses was carried out by Fedin & Govrilob (2002). The method was based on bead-on-plate welding. A CW CO_2 laser operated at an average power of 0.2 to 4 kW was used. A scanned welding velocity was maintained at 5–10 m/min. The focal depth into the material and focal length were 0.1 mm and 48 cm, respectively. The measured beam radius was 0.25 mm at the surface of the weld specimen. Guassian type intensity of the laser beam was $\sim 10^6$ W/cm^2. The resulting fusion zone shapes and KH dimensions were measured by optical microscopy.

3. Weld pool mechanism in laser welding

In general, both the shape and size of the KH during laser welding are dependent on process conditions. If stationary KH radius r_{kh} is small in comparison with the work piece thickness d and the travel speed is not too high, the KH can be approximated as a cylinder coaxial with the laser beam. It is shown that the cylindrical KH is held open and stabilized by pressure and energy balances described by Klein *et al* (1996). The pressure balance requires that the surface tension $p_\gamma = \frac{\sigma_{coeff}}{a}$ (σ_{coeff} is the surface tension coefficient) is compensated by the sum of the recoil

pressure p_{abl} of particles ablated at the KH surface and the excess pressure $\delta\rho_g$ due to gas flowing out of the KH. *a* represents line of contact of force. Taking into account the kinematic viscosity μ of the vapour, the average excess pressure $\delta\rho_g$ within the KH can be expressed (Kroos *et al* 1993).

$$\delta\rho_g = \frac{C_g\,(\mathrm{Re}_{0.7})}{3} \times \mathrm{Mg}^{0.7}\left(\frac{\delta}{r_{kh}}\right)^2 p_{abl}, \tag{1}$$

where C_g is the gas flow parameter, Re is Reynolds number, i.e., ratio of surface tension force and viscous force, Mg refers to Marangoni number which is proportional to surface tension force divided by viscous forces, δ is the melt thickness. Marangoni convection, also called surface-tension-driven convection or thermo-capillary convection, occurring in the weld pool, is of practical interest in welding. It can have a dramatic effect on the penetration depth of the resulting weld. The velocity obtained at pool surface due to outward surface flow is much faster than the inward return flow. These characteristic signatures are ascribed to Marangoni convection. This is pronounced while compared with gravity-induced convection. Increasing the beam power from 0.5 kW to 4 kW and reducing the beam diameter from 0.8 mm to 0.5 mm brings about stronger Marangoni convection. The latter, however, had a significantly greater effect. The surface flow is much stronger which renders return flow penetrate deeper into the weld pool. The surface temperature decreases with increasing radius, but not at a constant rate across the free surface. The surface temperature drops sharply near the edge of the laser beam but beyond this point, the decrease is marginal. This occurs especially when Marangoni convection is significant ($\mathrm{Mg} \geq 10^5$). In the presence of significant Marangoni convection, the calculated temperature field in the pool shows a very thin thermal boundary layer at the pool surface under the laser beam. In this case $\frac{\partial T}{\partial z}$ is very high within the boundary layer but much lower beyond it. The Marangoni number, which has been used widely as a measure for the extent of Marangoni convection, is a dimensionless number which is defined as

$$\mathrm{Mg} = -\frac{d\sigma}{dT}\frac{1}{\mu\alpha}V_{kh}\cdot\Delta T = \frac{-(\partial\gamma/\partial T)\,\Delta T\cdot V_{kh}}{\mu\alpha}, \tag{2}$$

where σ is the surface tension force, $\alpha = \frac{k}{\rho c_p}$ represents thermal diffusivity, the ratio of thermal conductivity to the volumetric heat capacity (ρc_p), $-(\partial\gamma/\partial T)$ is the temperature coefficient of surface tension, ρ and c_p are density and specific heat capacity, respectively, V_{kh} represents KH volume, ΔT is the temperature difference in the KH, μ refers to kinematic viscosity. The relaxational dimensionless parameter of KH melt motion τ can be calculated from various terms as mentioned below (Elizarova 2007):

$$\begin{cases} \tau = \dfrac{\mu}{\rho\,c^2}, \quad \text{or} \\[2mm] \tau = \dfrac{1}{\mathrm{Gr}}\dfrac{\beta\,g\Delta T\cdot(h_{kh})^2}{r_{kh}\,(V_c)^2} = \dfrac{\alpha}{\mathrm{Gr}}; \quad \mathrm{Gr} = \dfrac{\beta\,g\Delta T\,(h_{kh})^4}{r_{kh}\cdot\mu^2}, \quad \text{or} \\[2mm] \tau = \alpha\dfrac{\mathrm{Pr}}{\mathrm{Ma}\cdot(V_{kh})}; \quad \alpha = \left|\dfrac{\partial\sigma}{\partial T}\right|\cdot\Delta T\dfrac{1}{h_{kh}\,(V_c)^2}; \\[2mm] \mathrm{Pr} = \dfrac{\mu}{\alpha}; \quad \mathrm{Ma} = \dfrac{V_o}{V_c} \end{cases} \tag{3}$$

$$\mathrm{Ra} = \mathrm{Gr}\cdot\mathrm{Pr} = \frac{g\,\beta}{\mu\alpha}(T_s - T_\infty)\,h_{kh}, \tag{4}$$

where β is the volumetric thermal expansion coefficient, c is speed of sound, g is the acceleration due to gravity, Gr is Grashof number, h_{kh} and r_{kh} are depth and radius of KH, respectively, Pr and Ma represent Prandtl and Mach numbers, respectively, V_o and V_c represent object and sound velocity in the KH medium, respectively. The dimensionless coefficient of kinematic visocity μ, heat conductivity χ can be defined in terms of following expressions:

$$
\begin{cases}
\mu = \dfrac{1}{\text{Re}}\left(\text{Ma}^2 \cdot \Delta T\right); \\
\chi = \dfrac{\mu}{\text{Pr}\,(\gamma - 1)};
\end{cases}
\tag{5}
$$

where γ is the adiabatic coefficient. The curve of the KH bottom reduces due to surface tension force correspondingly to the depth profile. The KH evalution depend on the spatial and temporal amount of melt and melt motion. In case of low viscous melt, the melt moves directly towards the depth of the KH. It is unifrom across the radius of KH.

4. Result and discussion

In figure 2 phenomenological picture of KH front and rear wall is presented. KH has been formed due to interaction of CW CO_2 laser beam having Gaussian beam profile at the surface of material (Kumar *et al* 2010). In this figure, h_{kh} represents KH depth, W_{kh} is width of the KH at the half of maximum KH depth, KBH and KBM are KH bottom and KH mouth, respectively, r_{kh} is the radius of the KH mouth. Liquid–vapour mixed phases appear in front and rear walls of KH region where different hydrodynamical phenomena take place. These include Marangoni convection, hydrostatic force, vapour recoil pressure and thermocappilary force (Duley 1999; Kroos *et al* 1993; Kaplan 1994; Solana & Negro 1997; Xiao-Hu & Xi Chen 2002; Kumar *et al* 2007). In figure 2 FWKH and RWKH represent to front and rear wall of KH, respectively. The scale of RWKH liquid–vapour interface is lower than FWKH. In this case, the size of the KHM solid–liquid interface is more than the size of KHB solid–liquid interface. This occurs due to reduction in temperature profile prevailing in KHB region. This is linked to the quantity of melt flow in weld pool. It is assumed that the radius of KH is equal to the radius of the melt zone ($r_{kh} = r_{melt}$) at the mouth of KH. In both front and rear wall of KH solid–liquid interface scale decreases towards KH bottom. Where the length of melt pool is denoted by L_{wp}. This scale is higher at the rear wall of KH and increases significantly with higher specimen velocity due to motion of melt from front to the rear wall of KH. The length of weld pool significantly decreases with the depth of KH. L_{wp} is absent at the KHB. This happens for both front and rear walls of KH. This has been assumed that the beam radius is equal to the radius of vapour zone of the KH ($r_b = r_{kh}$). Melt convection appears in the front wall of KH which moves towards rear wall of KH and gets relaxed due to solidification process.

Figure 3 shows experimentally observed variation of KH depth and radius as a function of laser power. These values correspond to a constant welding speed of 8 m/min. In the dispensed laser power range 0.2–2.3 kW, the KH radius shows a small rise. It attains a constant value of 0.4 mm for laser power exceeding 2.3 kW. For laser power density ranging between 10^6 and 10^8 Wcm^{-2}, the radius of KH mouth is restricted to $1.7 \times r_b$, where r_b is beam radius. Figure 4 shows variation of super-sonic vapour flow velocity in the front wall of KH at various depths. This flow velocity attains a maximum value of 2.5 Ma at a KH depth of 3 mm. For KH rear wall, this maximum shifts to a value of 2.2 Ma. This occurs at a depth of 4 mm. For both front and rear walls of KH, the Mach number exhibits a decline after attainment of respective maxima. The
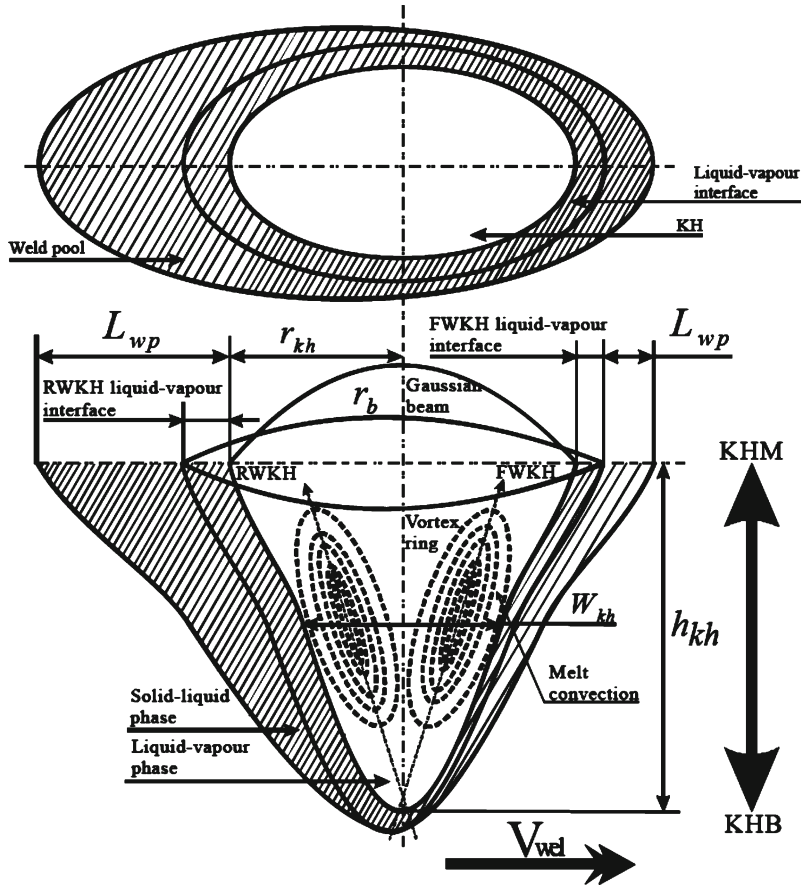
Figure 2. Keyhole phenomenological schematic with front and rear wall.

growth and relaxation trends exhibited by Mach number at front and rear walls of KH are similar except for the fact that there is shift in maximum value of Mach number in case of the latter. Figure 5 depicts variation of pressure at various KH depths. The curves pertain to front and rear KH walls (different trends are seen). In case of the rear wall, there is a maximum at 4 mm. The maximum corresponds to the maximum in fluid acceleration followed by decline due to flow dissipation occuring at KH depths of 4–5 mm. In front as well as rear walls, the KH surface does not move freely due to the presence of solid–liquid interface. Instead, the liquid film exerts pressure at this interface, which causes a local rise. This rise is continuous until a new equilibrium is reached. However, at the rear wall of KH, this surface is not constrained and can move away from the laser spot resulting in KH elongation studied by Aalderink *et al* (2007). Figure 5 shows the elongation of KH due to the presence of gradient in front as well as rear KH walls. Observations carried out during welding process reveal that, a circular KH while collapsing generates strong surface waves in the melt pool. In contrast, an elongated KH does not collapse due to pressure burst. This leads to rapid decline in surface waves causing formation of smooth weld bead after solidification of the melt pool. The results show that the holes are caused by collision of surface waves travelling over the surface of the melt pool. This happens on both front and rear
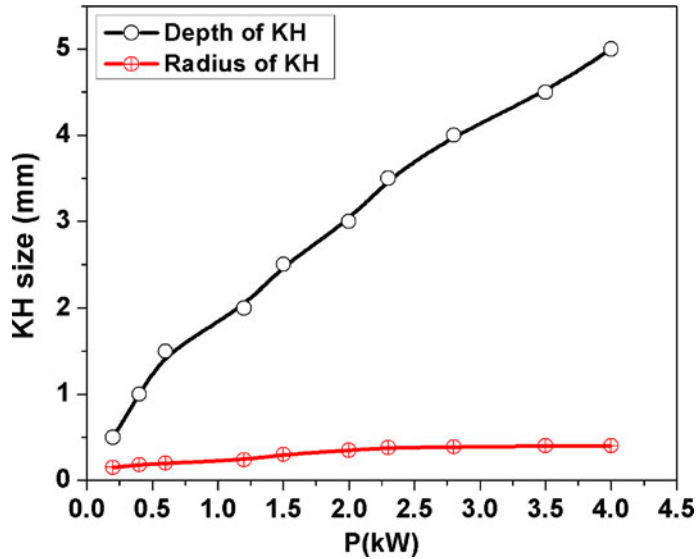
Figure 3. Keyhole size is a function of laser power.

walls of KH. Pressure induced KH collapse is frequent at KH depths 4–5 mm. Therefore, welding defects increase with the increasing KH length. Due to higher pressure gradient, Raleigh number is more pronounced around front wall as compared with the rear wall. This is shown in figure 6. For both the cases, flow of fluid is laminar in the KH region corresponding to 2–5 mm
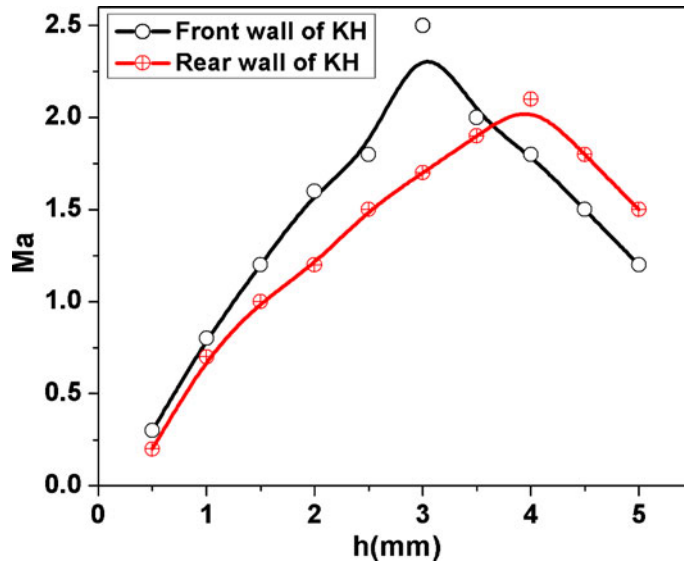
Figure 4. Mach number variation in the front and rear wall of KH depth.
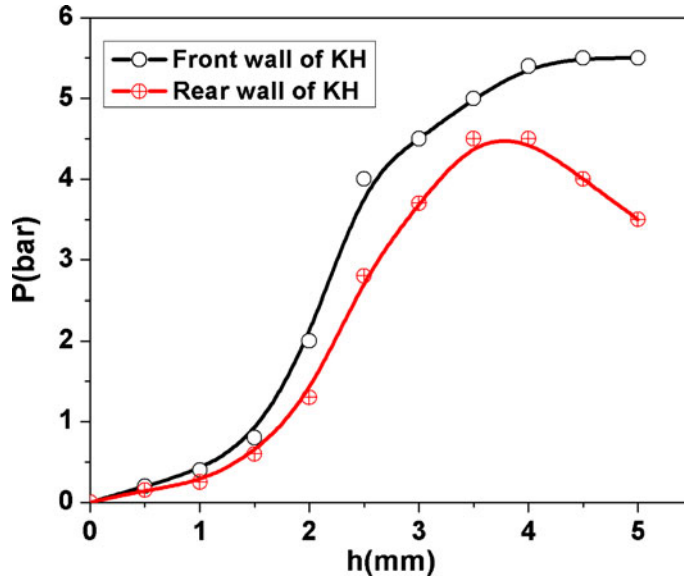
Figure 5. Pressure distribution in the front and rear wall of KH depth.

depths. Turbulent fluid motion present up to 2 mm KH depth below surface causes Raleigh number to have a value ranging between 2×10^8 and 2×10^9. Rapid solidification of the melt pool at KH depths 3–5 mm causes laminar flow patterns to appear. At this point, the Raleigh number consequently declines. In contrast, higher Raleigh number causes large oscillation amplitudes in melt pool surface waves causing KH collapse and splash generation. The weld pool oscillation
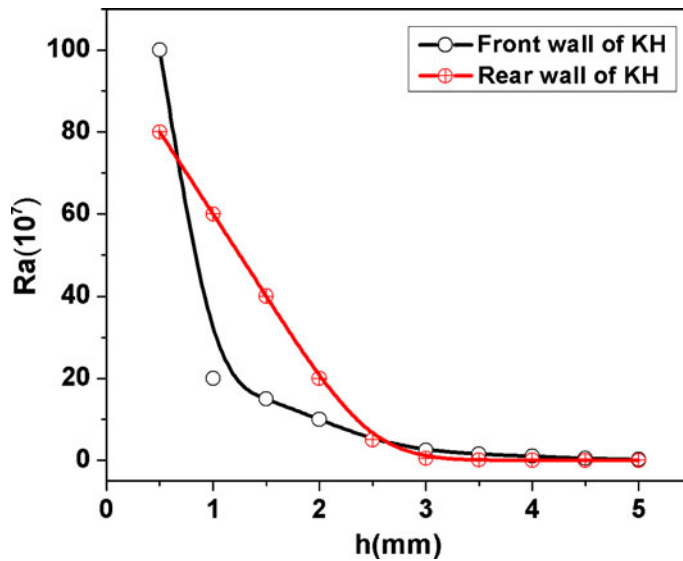
Figure 6. Raleigh number variation in the front and rear wall of KH depth.

arises from intermittent impingement of melt. Pulsation of the melt ejection can result in a number of weld defects such as material loss by splattering, variation in the penetration depth and uncontrollable transition from welding to cutting. Fluctuation in the evaporation fluxes across the front wall produces variation in the vapour pressure inside the KH. Consequently, the shape of the front and rear wall of KH changes significantly. This results in entrapment of vapour bubbles causing generation of porosity. In figure 7, it is shown that the ratio of Reynolds and Mach numbers (Re/Ma) is relatively higher in the region of 2–3 mm KH depth across the front wall of KH. The corresponding region of rear wall has a reduced value of Re/Ma. This reduction occurs due to significant relaxation in turbulent motion. In this connection, Marangoni convection, also called surface-tension-driven convection or thermo-capillary convection, in the weld pool assumes significance during laser welding. From the similarity principles of hydrodynamics, the Marangoni convection observed in the simulated weld pool can be expected to resemble the phenomenon occurring during laser welding practice (Tsai & Kou 1989; Oreper & Szekely 1984). Two counter-rotating cells appear in the meridian plane of the pool where the surface velocity exhibits a maximum. The outward surface flow is much faster than the inward return flow and centers of the cells near the pool edge experience higher ratio of Re/Ma. This is characteristic Marangoni convection. This mode dominates the pool as compared to gravity-induced buoyancy convection. Increasing the beam power and reducing the beam diameter will cause stronger Marangoni convection. Net effect of this convection is to replace cell centers closer to melt pool edge. However, displacing effects associated with buoyancy driven convection is always greater. Within the range of the experimental conditions, it is observed that increasing the beam power tends to reduce the depth of convection while reducing the beam diameter tends to increase it. The latter is attributed to increased momentum associated with reverse flow. In the KH depth between 1 and 1.5 mm, the convection is relatively higher at both front and rear wall of KH. This establishes the role of Marangoni number in mixed conduction–convection mode of heat transfer which prevails in the weld pool. Due to this, the consequential ascendancy of
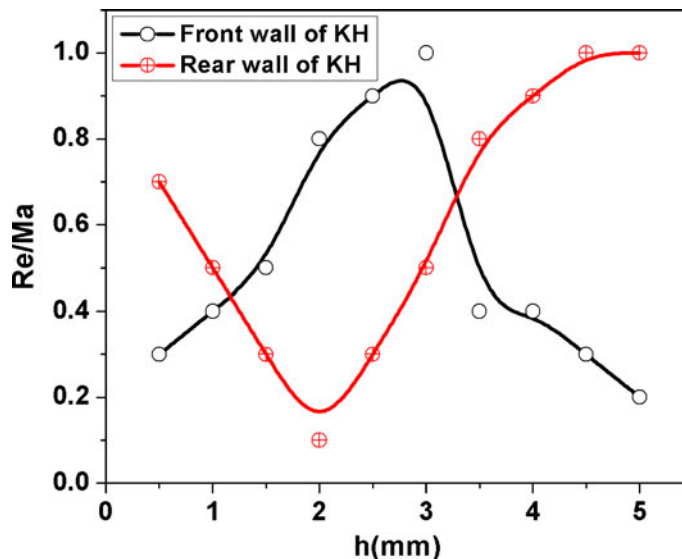
Figure 7.   Ratio of Re/Ma as a function of KH depth.

Marangoni number becomes quite significant. Higher the Marangoni number, the stronger is the Marangoni convection and higher is the maximum outward surface velocity of the weld pool. Strong Marangoni convection has been observed through flow visualization in a simulated weld pool of 10 mm in diameter, where Marangoni was around 2×10^4 (Limmaneevichitr & Kou 2000). Since the associated Peclet number is also high, heat transfer in liquid pool is dominated by Marangoni convection. If the KH formation time is comparable to or higher than the beam radius divided by the sample translation velocity, then the KH permanently remains in the state of growth. In this case, the KH axis deviates from the beam axis and the KH shape becomes asymmetric. Melt ejection from the beam-melt interaction area results in the forward movement of the front part of KH into the material. The melting front also moves together with the KH wall and a new portion of the metal gets melted to replace the ejected mass. This is a distinctive feature in high power LBW. The reported models analysing laser spot welding process had often considered purely conduction mode of heat transfer in weld pool and the surrounding solid substrate (He *et al* 2003). The results make it possible to prevent the characteristics of the welding zone and give an estimation of the capillary diameter of the weld pool (Kamel *et al* 2008). Laser intensity absorbed on the keyhole walls with the heat flux lost, the mechanism of energy balance on the keyhole walls was investigated (Xiang & Li 2003). The recoil pressure associated with energetic evaporation is sufficient to produce a deep, narrow depression in the molten material present underneath. While high recoil pressure is exerted on the KH, especially at the bottom, it is not sufficient to eject the melt entirely out of the cavity because the upward flow momentum from the KH bottom is reduced by the viscous shear stress on the KH wall. The ejected amount of vapour flow is significantly higher across front wall of the KH compared to the rear wall. The physical mechanisms that are considered in the present modelling as responsible for the KH collapse are based on surface tension, buoyancy force, recoil pressure and vapour flow friction. The surface tension increases when the temperature decreases and reaches minimum at the melt pool periphery. It has minimum value near the KH aperture.

5. Conclusion

Experimental and analytical results explain significant increase in KH depth during LBW of Al 1100 alloy. However, the radius of the KH mouth remains constant in the laser power ranging between 2.8 and 4.0 kW. It is found that the KH depth is proportional to the laser power for a welding speed of 8 m/min. The trend in growth of Mach number variation is symmetrical for both front and rear walls of KH. The Mach number has a higher value at front wall of KH. This maximum is attained at centre of KH axis. However, with regard to rear wall of KH, the corresponding value of Mach number is not only reduced, but also displaced farther down to the KH bottom. At the KH bottom, maximum value of Mach number arises due to enhanced defferential pressure bursts occurring with higher frequencies. This is around 4.5 bar at the 4 mm KH depth. After this, the Mach number suddenly declines due to pressure dissipation. Turbulence in the melt-vapour manifests in the KH bottom region of 0–2 mm. The corresponding Raleigh number ranges between 2×10^8 and 2×10^9. The rapid decline of the Raleigh number in the KH region located between 3 and 5 mm for both front and rear wall of KH is attributed to the laminar flow of the melt-vapour. Re/Ma ratio is significantly high at KH depth of 2–3 mm in the case of front wall of KH. In contrast with this, at similar location pertaining to the rear wall of KH, Re/Ma ratio depicts a minimum. Such a reversal is brought about by Marangoni convection. Higher Marangoni convection always brings out rapid melt-vapour motion in weld pool. This is intimately related to the dispensed laser power density.

Acknowledgements

Symbols

r_{kh}	Keyhole radius
σ_{coeff}	Surface tension coefficient
p_{abl}	Ablation pressure due to recoil pressure
$\delta\rho_g$	Excess pressure due to gas flowing
μ	Kinematic viscosity
C_g	Gas flow parameter
Re	Reynolds number
Mg	Marangoni number
δ	Melt thickness
σ	Surface tension force
α	Thermal diffusivity
ρc_p	Ratio of thermal conductivity to volumetric heat capacity
$-(\partial\gamma/\partial T)$	Temperature coefficient of surface tension
ρ	Melt density
c_p	Specific heat capacity
V_{kh}	Keyhole volume
ΔT	Temperature difference in the keyhole
τ	Relaxational dimensionless parameter
β	Volumetric thermal expansion coefficient
c	Speed of sound
g	Acceleration due to gravity
Gr	Grashof number
h_{kh}	Depth of keyhole
Pr	Prandtl number
Ma	Mach numbers
Nu	Nusselt number
V_o and V_c	Object and sound velocity in keyhole medium
χ	Heat conductivity
γ	Adiabatic coefficient
Pe	Peclet number
Ra	Raleigh number
r_b	Beam radius
FWKH	Front wall of keyhole
RWKH	Rear wall of keyhole
V_{wel}	Spacimen velocity
W_{kh}	Width of keyhole at half of maximum depth
Lwp	Length of weld pool

References

Aalderink B J, de Lange D F, Aarts R G K M and Meijer J 2007 Keyhole shapes during laser welding of thin metal sheets. *J. Phys. D: Appl. Phys.* 40: 5388–5393

De A, Walsh C A, Maiti S K and Bhadeshia H K D H 2003 Prediction of cooling rate and microstructure in laser spot welds. *Science and Technology of Welding and Joining* 8: 391–399

Duley W W 1999 *Laser welding*. New York: Wiley Interscience

Elizarova T G 2007 *Quasi-gasdynamic equation and numerical methods for viscous flow simulation*. Moscow Scientific world, 1–352

Fabbro R, Slimani S, Coste F and Briand F 2005 Study of keyhole behaviour for full penetration Nd–Yag CW laser welding. *J. Phys. D: Appl. Phys.* 38: 1881–1887

Fedin A B and Govrilob A A 2002 *Laser welding experiment*. Private communication

He X, Fuerscbach P W and DebRoy T 2003 Heat transfer and fluid flow during laser spot welding. *J. Phys. D: Appl. Phys.* 36: 1388–1394

Kamel A, Wacef B S, Hatem M, Georges L and Michel A 2008 Modelling of CO2 laser welding of magnesium alloys. *Opt. Laser Technol.* 40: 581–588

Kaplan A A 1994 Model of deep penetration laser welding based on calculation of the keyhole profile. *J. Phys. D: Appl. Phys.* 27: 1805–1814

Klein T, Vicanek M and Simon G 1996 Forced oscillations of the keyhole in penetration laser beam welding. *J. Phys. D: Appl. Phys.* 29: 322–332

Kroos J, Gratzke U, Vicanek M and Simon G 1993 Dynamic behaviour of the keyhole in laser welding. *J. Phys. D: Appl. Phys.* 26: 481–486

Kumar N, Dash S, Tyagi A K and Baldev Raj 2007 Hydrodynamical phenomena in the process of laser welding and cutting. *Science and Technology of Welding and Joining* 12: 540–548

Kumar N, Kataria S, Shanmugarajan B, Dash S, Tyagi A K, Padmanabham G and Baldev Raj 2010 Contact mechanical studies on CW CO$_2$ laser beam weld of mild steel with ambient and under water medium. *Materials and Design* 31: 3610–3617

Lee J Y, Sung H K, Farson D F and Choong D Y 2002 Mechanism of keyhole formation and stability in stationary laser welding. *J. Phys. D: Appl. Phys.* 35: 1570–1576

Limmaneevichitr C and Kou S 2000 Flow visualization of Marangoni convection in weld pools. *Weld Journal* 79: 126–135

Oreper G M and Szekely J 1984 Heat and fluid-flow phenomena in weld pools. *J. Fluid Mech.* 147: 53–79

Solana P and Negro G 1997 A study of the effect of multiple reflections on the shape of the keyhole in the laser processing of materials. *J. Phys. D: Appl. Phys.* 30: 3216–3222

Trivedi A, Bag S and De A 2007 Three-dimensional transient heat conduction and thermomechanical analysis for laser spot welding using adaptive heat source. *Science and Technology of Welding and Joining* 12: 24–31

Tsai M C and Kou S 1989 Marangoni convection in weld pools with a free surface. *Int. J. Numer. Methods Fluids* 9: 1503–1516

Xiang Z J and Li J L 2003 A conduction model for deep penetration laser welding based on an actual keyhole. *Opt. Laser Technol.* 35: 5–12

Xiao-Hu Ye and Xi Chen 2002 Three-dimensional modelling of heat transfer and fluid flow in laser full-penetration welding. *J. Phys. D: Appl. Phys.* 35: 1049–1056